This is the post print version of the article, which has been published in
European Polymer Journal. 2019, 118, 78-87.
https://doi.org/10.1016/j.eurpolymj.2019.05.041

Porous polybutylene succinate films enabling adhesion of human embryonic stem cell-derived retinal pigment epithelial cells (hESC-RPE)

M. Teresa Calejo[1]*, Anne Haapala[1,2], Heli Skottman[2], Minna Kellomäki[1]

[1] BioMediTech, Tampere University, Tampere, Finland

[2] BioMediTech, Tampere University, Tampere, Finland

* Corresponding author. E-mail: teresa.rebelocalejo@tuni.fi; +358 50 301 4048

Abstract

In the last decade, several studies have shown that polybutylene succinate (PBSu) has a high potential as a biomaterial enabling cell adhesion and growth. In this study, porous PBSu films have been prepared by the breath figure method (BF) and by particulate leaching (PL), and characterized in terms of thickness, surface properties, diffusion capacity and in *vitro* stability. Because porous films are of high interest for tissue engineering of retinal pigment epithelium (RPE), the initial viability and adhesion of human embryonic stem cell-derived RPE onto the PBSu films was then evaluated. To the best of our knowledge, this is the first study on the adhesion behavior of hESC-RPE onto porous and biodegradable polymer surfaces. The results clearly demonstrated that the two manufacturing methods produced materials with very distinct properties. Films produced by BF expressively demonstrated the highest roughness and surface area, and the lowest water contact angle. These features likely contributed to increase the biocompatibility of the surface, particularly when coated with laminin and collagen IV, as observed by the improved cell viability, cell morphology, adhesion and production of extracellular matrix proteins. Altogether, our results showed not only that PBSu holds high potential in retinal tissue engineering, but also that the physical properties and biocompatibility of the material are highly dependent on the adopted casting method.

1. Introduction

High porosity in biomaterials used for tissue engineering is essential to ensure the delivery of nutrients and oxygen to cells, and to prevent the accumulation of waste products around the growing tissue. In addition, the presence of pores on the surface of the biomaterial, as well as their size and distribution, can significantly affect the way cells attach to the surface and how they migrate and proliferate on the surface and into the scaffold [1]. Porous/patterned films can be prepared by a variety of methods, including photolithography, soft lithography, colloidal lithography, chemical vapor deposition, to name a few, but most of them require expensive and specific equipment [2,3]. The breath figure (BF) method is a simple, inexpensive and somewhat versatile alternative to prepare thin, porous and micro/nanopatterned films via solvent casting under high air humidity [4,5]. Furthermore, the method is fast, enables the preparation of multiple samples in one experiment, and allows a precise control of pore size and shape through manipulation of process parameters [5,6]. Over almost two decades, several researchers have shown the potential of the so-called 'honeycomb films' prepared by BF as substrates for e.g. cardiomyocytes, chondrocytes, osteoblasts, stem cells, mast cells, endothelial cells, hepatocytes, fibroblasts, and keratinocytes [3]. Noteworthy is that this specific topography seems to affect not only cell adhesion, but also cell morphology, migration, differentiation and gene expression, as discussed in our recent review [3]. Additionally, our team has recently shown that honeycomb films based on 96/4 L-lactide/D-lactide (PLDLA) can be used to tissue engineer retinal pigment epithelial cells (RPE) [7,8]. Thin biomaterials are promising candidates as substrates for RPE cell replacement in patients suffering from degenerative eye diseases such as age-related macular degeneration (AMD), which are characterized by the progressive loss of RPE. In severe disease cases, the supporting layer of RPE – the Bruch's membrane – is also damaged, and the thin biomaterial becomes a crucial replacement, providing the necessary support for the regenerating RPE [7,8]. In this case, the presence of a porous structure is especially important, since it is essential to ensure the efficient transport of nutrients, ions, water, oxygen and waste products between photoreceptor cells and the choriocapillaris when the epithelium is transplanted [9].

Polybutylene succinate (PBSu, Figure 1) is an aliphatic polyester that has been attracting interest in the fabrication of biomedical implants. PBSu is biodegradable, originating nontoxic degradation products, and it has excellent processability, mechanical and thermal properties [10]. Biomaterials based on PBSu have, for example, shown promise as substrates inducing bone cell growth [11,12] and differentiation of human mesenchymal stem cells [13]. Porous PBSu-based biomaterials have been prepared by knitting [13,14], typically being hundreds of millimeters-thick, and having large pores (pore size ~70 µm, thickness 700 µm). Alternatively, porous PBSu scaffolds have been prepared by solvent casting and particulate leaching (PL), where large particles (e.g. 300-500 µm) are used as the porogen species [11,12,15]. In spite of the potential of such biomaterials as scaffolds for e.g. bone or cartilage tissue engineering, they are largely unsuitable for tissue engineering of RPE, where small pore size (< 5-10 µm) is essential to prevent cell migration across the material, and low thickness is needed if transplantation to the subretinal space is considered.

In this work, the BF method was used, for the first time, to prepare porous PBSu films as substrates for human embryonic stem cell-derived RPE (hESC-RPE). As an RPE cell source, hESCs are uniquely advantageous since they can be indefinitely expanded, while the differentiated cells resemble more closely the native epithelium than the immortalized cell lines [16]. A number of authors have developed artificial membranes for culture of RPE [17–20], including hESC-derived [8,21–23], where long-term cultivation is typically carried out to investigate the maturation and functional aspects of the cells. In spite of this, the adhesion behavior of hESC-RPE has been very scarcely studied and, to the best of our knowledge, no studies have been published describing the adhesion of hESC-RPE onto patterned substrates. Here, prepared PBSu films prepared by BF were compared to equivalents prepared by PL in terms of thickness, surface topography, electrical resistance through the material, water contact angle and *in vitro* stability. Due to anchorage being a critical process for retinal pigment epithelial cells, our work also provides preliminary data concerning the adhesion of hESC-RPE onto the PBSu films, with focus being given to the investigation of the influence of surface topography on the early stages of cell adhesion.

Keywords

Polybutylene succinate; biodegradable films; breath figures; retinal pigment epithelium; cell adhesion

2. Materials and Methods

2.1. Film preparation by the BF method

Films prepared by the BF method (hereafter designated 'PBSu BF', Table 1) essentially followed the procedure described in our previous work [7,8] with slight modifications. PBSu pellets (Bionolle 1020 MD, Showa Denko, Japan) were dissolved in chloroform overnight. A 2% (w/v) PBSu solution containing 5% 1,2-dioleoyl-sn-glycero-3-phosphoethanolamine (DOPE, TCI Chemicals, Japan) was thereafter prepared in chloroform. The solution was left to rest for an hour before being cast (0.5 ml) on a glass petri dish (⌀ 40 mm, Steriplan®). Solvent evaporation took place under vertical humid airflow (80 ± 5% relative humidity) at room temperature (RT). Finally, films were repeatedly rinsed with 70% ethanol in order to remove the surfactant from the material, and were left to dry at RT. Samples were stored in a vacuum chamber until further use. For comparison, control samples were similarly prepared in the absence of surfactant ('PBSu BF Ctr', Table 1).

Table 1. Samples and controls prepared in this work.

Sample	[PBSu] (%)	[DOPE] (%)	Sucrose microparticles (%)
PBSu BF	2	5	-
PBSu BF Ctr	2	-	-
PBSu PL	2	-	5
PBSu PL Ctr	2	-	-

2.2. Film preparation by the particulate leaching (PL) method

For the preparation of porous films by PL (henceforth designated 'PBSu PL', Table 1), a suspension containing sucrose particles as porogen (particle size = 1-3 μm) was initially prepared in chloroform. In order to prevent the presence of large particle aggregates, the suspension was exposed to two consecutive cycles of sonication in an ultrasound bath (30 min) and magnetic stirring (30 min). After the sonication and mixing cycles, the particle suspension was left to stand for 60 minutes so that any remaining large aggregates would be let to sink to the bottom of the vial. Then, the supernatant of this suspension was mixed with the PBSu solution to form a solution with a specific polymer and sucrose concentration (Table 1). The solution was cast onto a glass petri dish (0.5 ml), as described above, and the solvent was let to evaporate at room temperature and at room (30-40%) humidity. After complete solvent evaporation, films were rinsed with distilled water and then left to soak in 4 ml of distilled water for 24h in order to ensure dissolution and elimination of the sucrose particles. Distilled water was changed twice during this process. Films were finally left to dry at RT, before being placed in a vacuum chamber (thus ensuring complete water elimination) until further analysis. For comparison, control films (hereafter designated 'PBSu PL Ctr', Table 1) were similarly prepared in the absence of porogen.

2.3. Film characterization

2.3.1. Film thickness and surface topography

Film thickness was estimated using a digital micrometer (Mitutoyo, Japan). In order to obtain a quantitative value representative of sample homogeneity (as reflected by the standard deviation values), thickness was measured on 3 different areas of the same sample, in a total of 6 replicates per sample type.

The surface topography of the films was analyzed by atomic force microscopy (AFM) using an XE-100 AFM from Park Systems Corp, USA. Samples were scanned in noncontact mode (scanning area 40 μm x 40 μm), under air and at RT, using an APPNANO AFM cantilever (type ACTA, L = 125 μm, tip radius < 10 nm, f = 200-400 kHz, spring constant = 25-75 N m^{-1}, coating aluminium). Acquired data was analyzed using Park Systems image analysis software (XEI, Park Systems, USA). The arithmetic means of surface

roughness (R_a) and surface area (SA) were determined from a minimum of three randomly chosen images using XEI software. AFM images were further analyzed with Image J software (available at https://imagej.nih.gov/ij/), in order to estimate average pore size at the surface of the materials (n=100).

2.3.2. Electrical resistance through the films

The diffusion of ions across the films was assessed by measuring the electrical resistance (R), essentially as described in our previous work [7,8]. Samples and controls were mounted into P2307 sliders (Physiologic Instruments, USA) and tightly assembled to a custom-built Teflon chamber. Sliders were submerged in Dulbecco's phosphate-buffered saline (DPBS), and R values across the materials were monitored using a Millicell electrical resistance system volt-ohm meter (Merck Millipore, Germany). Three independent measurements were made for each sample.

2.3.3. Water contact angle (WCA)

Static water contact angles were measured at RT using the sessile drop method in a Theta Lite optical tensiometer (Attension, Biolin Scientific AB, Sweden). Measurements were carried out using deionized water. Average values were calculated from the left and right angle values, and from a total of four replicates per sample. In addition, measurements were carried out at 0s, 6s and 12 s after deposition of the water drops.

2.3.4. Hydrolytic stability of PBSu films

The *in vitro* hydrolytic stability of PBSu films was assessed by incubation of samples at 37 °C in 0.5 M TRIS-buffer (pH 7.4) for 2, 4, 8 and 16 weeks. The initial weight (m_i) of the samples (1 cm x 1 cm) was registered before incubation. The buffer solution was replaced weekly. At each time point, three replicates of each sample type were collected, washed with distilled water, and the excess water removed with tissue paper before measuring the wet weight (m_w). Samples were thereafter placed in a vacuum chamber to dry,

and the dry weight (m_d) was registered. The mass retention % was calculated from the following equation: $\text{Mass retention (\%)} = \frac{m_d}{m_i} \times 100$.

The surface topography of the dry samples collected at each time point was further analyzed by AFM with estimation of surface roughness (n=4), as described above.

2.4. Sterilization of samples and dip-coating with extracellular matrix (ECM) proteins

Samples (7 mm x 7 mm) were exposed to UV light (20 min), disinfected with 70% ethanol (10 min) and washed three times with sterile DPBS. Cells were seeded onto both uncoated PBSu films, and on dip-coated samples, placed inside 48-well plates (well size 1.1 cm^2). Dip-coating was carried out by sample immersion (4°C, overnight) in 200 µl/well of DPBS supplied with $CaCl_2$ and $MgCl_2$ and containing collagen IV (from human placenta, Sigma-Aldrich, USA) and laminin 521 (Biolamina, Sweden). Collagen and laminin content in the solution was respectively 10 and 0.75 $\mu g.cm^{-2}$. The unbound protein was removed by washing the samples twice with the buffer solution (300 µl/well) and with the cell culture medium (300 µl/well). Uncoated samples were treated with DPBS, in the absence of proteins.

2.5. Human embryonic stem cell-derived retinal pigment epithelial cells (hESC-RPE)

The culture and characterization of human embryonic stem cell (hESC) line Regea 08/017 (46,XX) as well as RPE differentiation were conducted as previously described [24,25]. hESC cells were cultured and differentiated using serum-free conditions [26]. Briefly, hESCs were cultured on top of mitomycin (10 µg/mL; Sigma-Aldrich, USA)-treated human foreskin fibroblast feeder cells (CRL-2429TM; ATCC, USA), using knockout Dulbecco's modified Eagle's medium supplemented with 20% Knock-Out Serum Replacement (KO-SR), 2 mM Glutamax-I, 0.1 mM 2-mercaptoethanol (all from Life Technologies, USA), 1% nonessential amino acids, 50 U/m penicillin/streptomycin (both from Lonza Group Ltd., Switzerland), and 8 ng/mL human BFGF (Peprotech, UK). Spontaneous differentiation of hESCs into RPE cells was induced in floating cell aggregates by reducing the KO-SR concentration to 15% and removing the bFGF from the

hESC culture medium (RPE basic medium)[24]. The pigmented areas were then isolated manually using a scalpel, dissociated with Tryple Select (Life Technologies, USA), and seeded on well plates, previously dip-coated with collagen IV from human placenta (Sigma-Aldrich, USA) at a concentration of 5 μg/cm^2. The differentiated RPE cells were seeded on the uncoated and dip-coated PBSu films at a density of 1.8 x 10^5 cells.cm^{-2}. Cells were cultured on the materials for 1 and 5 days, in order to assess cell adhesion to the film surface. The RPE basic medium was changed on days 1 and 2.

2.5.1. Cell viability/proliferation

Cell viability was assessed at 1 and 5 days using PrestoBlue™ reagent (Thermo Fisher Scientific, USA), according to the manufacturer's instructions. Briefly, the reagent was mixed with the culture medium in a ratio of 1:10 (v/v). Cells were then incubated for 30 min at 37°C with this reagent solution, after which volumes of 100 μl per well were sampled and replaced with fresh medium. Plain medium and PrestoBlue mixture without cells were used as controls. The fluorescence intensity was measured in a 96-well plate using the Wallace Victor2™ 1420 Multilabel counter (Perkin Elmer Wallace, USA), using an excitation wavelength of 544 nm and an excitation wavelength of 615 nm. Two measurements were made for each well, and the average cell viability was calculated from the results of 4 independent replicates per time point.

2.5.2. Protein staining/immunofluorescence studies

The expression and localization of collagen type IV, laminin, fibronectin and vinculin by hESC-RPE were investigated by immunofluorescence staining after 1 and 5 days of culture. Films were washed with phosphate buffer saline (3 x 5 min). Cells were then fixed with 4% paraformaldehyde (10 min) and were washed again with the buffer solution (3 x 5 min). Cell permeabilization was induced by adding 300 μl 0.1% Triton X-100 in phosphate buffer saline to each sample (10 min, RT). Background interference was minimized by blocking with 3% bovine serum albumin protein (BSA) in the buffer solution (1 h, RT). After washing three times with phosphate buffer saline, samples were incubated (overnight, 4°C) with 0.5% BSA-

phosphate buffer saline containing the primary antibodies, specifically: mouse anti-collagen IV (Millipore, USA, dilution 1:200), rabbit anti-laminin (Abcam, UK, dilution 1:100), rabbit anti-fibronectin (Abcam, UK, dilution 1:500) and rabbit anti-vinculin (Sigma-Aldrich, USA). Samples were then washed with the phosphate buffer saline solution (3 x 5 min, RT), and incubated (1h, RT) with the solutions containing the secondary antibodies: donkey anti-rabbit Alexa Fluor 488 (1:800, Molecular Probes, UK) and goat anti-mouse Alexa Fluor 568 (1:800, Molecular Probes, UK). Secondary controls were prepared to account for unspecific binding of secondary antibodies. Two replicates of the PBSu films were prepared for each staining combination. Finally, samples and controls were washed as before with the buffer solution, and were mounted onto glass slides using VectaShield mounting medium with DAPI (Vector Laboratories, Switzerland) for nuclei visualization.

For observation of filamentous actin, cells were fixed and permeabilized as described above, and were afterward incubated at RT for 20–30 min with phalloidin-tetramethylrhodamine B isothiocyanate (TRITC, Sigma–Aldrich, USA) diluted 1:300 in 3% BSA in DPBS. Samples were washed with this buffer solution (3 x 5 min) before being mounted in the Vectashield mounting medium containing DAPI for nuclei observation.

Images were taken using a LSM780 Confocal Microscope (Olympus, Japan), using a 63× oil immersion objective lens. The images were analyzed using ZEN Black lite software (Carl Zeiss, Germany).

2.5.3. Statistical analysis

All numerical data are shown as mean and standard deviation. Electrical resistance and thickness data was analyzed using a one-way ANOVA and Games-Howell post hoc test. Water contact angle data was analyzed using a one-way ANOVA and the Tukey post hoc test. Mass change data in the hydrolysis experiment were compared to the initial mass of each sample using a one-way ANOVA and using either the Tukey or the Games-Howell post hoc tests. Cell proliferation data was analyzed similarly, or using the Mann–Whitney U-test.

3. Results and discussion

3.1. Surface morphology of PBSu films

PBSu-based biomaterials have been increasingly studied, and the results generally suggest that this aliphatic polyester holds high potential as a biomaterial in a variety of biomedical applications [27]. Typical methods used to prepare PBSu films include hot compression-moulding [28–30] and injection moulding [31,32], but these methods fail to introduce porosity onto the materials, which is a crucial property of substrates intended for tissue engineering applications. The breath figure method (BF) has been widely employed to prepare films with highly organized surface porosity[3]. Such honeycomb films have been prepared by BF using various polymers, including e.g. polycaprolactone (PCL) [33], poly(lactic-co-glycolic acid) (PLGA) [34], poly(lactic acid) (PLA) [35], polystyrene [36] and several copolymers [37–39] and blends [40]. In this work, we intended to demonstrate, for the first time, the feasibility of using this method to prepare homogeneous PBSu films with a regular surface porosity, with the ultimate aim of creating thin and permeable materials for tissue engineering applications, exemplified here as substrates providing support to the adhesion of hESC-RPE.

The solvent casting/particulate leaching (PL) method is a commonly used method to prepare porous scaffolds, which involves the incorporation of water-soluble particles in the polymer solution. Following casting and drying, a washing step is employed to remove the particles from the material, leaving the open pores. In spite of its simplicity, drawbacks include the heterogeneous distribution of particles in the material, and the difficult removal of the particles when a dense layer of polymer is formed around them [41]. The PL method is also typically employed to create large pores on thick materials [11,12,15]. Due to its common use, the PL method was chosen here in an attempt to prepare thin, porous films, and in order to establish differences with the materials prepared by BF. Even so, the literature is scarce in terms of the production of thin films using small porogen particles (1-2 µm), as carried out in our work.

PBSu BF films prepared in the presence of the surfactant DOPE were macroscopically homogeneous. Microscopically, these samples demonstrated a homogeneous presence of pores at the surface (3.21 ± 0.37

μm) created by the humid air flow during solvent evaporation. Pore arrangement was regular, demonstrating in some regions a honeycomb-like morphology, as shown in Figure 2. These conditions also resulted in samples with high surface roughness (R_a) and high surface area (SA, Table 2). Conversely, samples prepared in the absence of the surfactant were macroscopically heterogeneous and were characterized by heterogeneous pore distribution at the surface (Figure 2). In fact, the surface of PBSu BF Ctr contained large areas with small pores (1.51 ± 1.32 μm), and smaller areas with significantly larger pores (up to 50 μm), which further resulted in a heterogeneous distribution of R_a and SA values (Table 2).

Table 2. Surface roughness and surface area of PBSu films.

Sample	Roughness (R_a, μm)	Surface area (μm^2)
PBSu BF	0.660 ± 0.096	2820 ± 44
PBSu BF Ctr	0.301 ± 0.138	2100 ± 103
PBSu PL	0.150 ± 0.001	1896 ± 12
PBSu PL Ctr	0.137 ± 0.003	1869 ± 22

The surface of PBSu PL films was found to be significantly smoother (Figure 2, Table 2) than the surfaces of films prepared under high humidity. Samples prepared by this method also contained small, randomly disposed pores, with an estimated pore diameter of 1.34 ± 0.52 μm. Surface area, as well as average pore diameter (1.32 ± 0.50 μm) were very similar to those obtained for the control (PBSu PL Ctr). However, the presence of the porogen caused a modest but statistically significant increase in surface roughness as compared to the control. These results suggest that the obtained surface topography of samples prepared at room humidity is a result of both the random arrangement of the polymer chains, and, in the case of PBSu PL, also by particulate leaching from the surface.

3.2. Film thickness and electrical resistance

Film thickness was considered an essential feature during material optimization for various reasons. First of all, differences in thickness between different areas of the each film (and respective standard deviation values) are representative of the spreading uniformity of the polymer solution during casting on the glass

surface, as well as of the homogeneity of inter- and intra-molecular aggregation of polymer chains. In the event of transplantation of RPE to the back of the eye, the material, serving as a 'prosthetic Bruch's membrane', should also be as thin as possible (though handleable enough for surgical implantation), in order to fit the space between the photoreceptors and the choroid, ensuring the diffusion of molecules between these tissues. Thin films are also expectedly more permeable than thick films, thereby facilitating the passive diffusion of molecules, oxygen, ions and waste products, which is essential both *in vitro* and *in vivo* [42].

The right vertical axis in Figure 3 denotes the average thickness of PBSu films (triangular markers). The standard deviation values are indicative of the heterogeneity of the formed films. Average thickness values for PBSu BF (prepared in the presence of DOPE) and PBSu BF Ctr (prepared in the absence of surfactant) were 17.9 ± 3.5 and 38.5 ± 18.0 μm, respectively. The significantly ($p < 0.05$) thicker control sample was also shown to be highly heterogeneous, as shown by the large distribution of thickness values among replicates. Conversely, PBSu BF was the sample with the smallest standard deviation, suggesting that this was the most homogeneous sample in terms of thickness. Thickness (as well as porosity) of polymer films prepared by the BF method is known to be affected by a variety of factors such as the solvent, the polymer concentration, and the humidity and temperature in the environment [43]. In addition, both the uniformity of the microporous films and the wall thickness are affected by the interfacial tensions between the water droplets and the chloroform solutions [44]. For the preparation of polylactide-based honeycomb films, DOPE has been shown to be a very effective surfactant, maintaining a high interfacial tension during film formation and thereby enabling the formation of a well-organized array [45]. In this work, thickness results point out in the direction of DOPE inducing the expansion of the polymer solution on the glass surface, causing the polymer to be homogeneously distributed, as discussed above, and forming thinner PBSu films. PBSu PL films, as well as the control samples prepared in the absence of porogen (PBSu PL Ctr), had an average thickness of approximately 20 μm (Figure 3), indicating that the presence of the sucrose particles did not significantly affect the thickness of the samples.

The diffusivity of small ions through the pores was assessed by measuring the electrical resistance (R) across the materials. In our previous research [7,8], we discussed that the determination of R can be a simple, fast and cost-effective means to assess the diffusion capacity of porous membranes, and that R inversely correlates with the permeability across the material, i.e. lower R implying higher permeability. Results for R measurements are shown as columns in Figure 3 (left vertical axis). PBSu BF Ctr was, again, the most divergent sample among all, showing the lowest value of R, i.e. the largest diffusion capacity across the film. This can be explained by the fact that very large pores (up to 50 µm) coexist with much smaller pores (1-2 µm, Figure 2), which is furthermore consistent with the heterogeneous nature of the film across the z-direction (as assessed by the large standard deviation in the thickness measurements). Average R values estimated for PBSu BF were the second lowest, suggesting an increased flow of ions through this material. Even so, differences between PBSu BF, PBSu PL and PBSu PL Ctr did not reach statistical significance ($p < 0.05$), which may be due to the similar thickness of these samples. Moreover, the similar results observed for the samples cast at room humidity (PBSu PL and PL Ctr) in terms of surface topography (Figure 2), thickness and, more importantly, R (Figure 3) , suggest that the presence of the sucrose particles was not sufficient to improve the bulk porosity of the materials, and thereby the diffusion across them. This observation is likely related with the packed arrangement of the polymer molecules in the matrix, preventing the exposure of the inner porous structure, and/or with the difficult removal of the sucrose particles, which, as mentioned previously, is one of the most common disadvantages of the PL method [41].

Again, it is important to emphasize that materials developed as substrates for hESC-RPE should not hinder the free flow of nutrients, oxygen, ions and waste products, which means that R should be as low as possible. Mature hESC-RPE cells typically form a tight epithelium, and values of R measured across the cell layer can reach values of ~300 $\Omega.cm^2$ [24]. The fact that, in our work, values of R were always at least 3.5 times lower than the value of R for mature hESC-RPE, suggests that the materials will not be the diffusion-limiting factor, but rather the epithelium itself. Even so, future permeability experiments may reveal important information concerning the molecular cutoff range of the PBSu films.

3.3. Water contact angle

The results for the WCA of PBSu films measured 0, 6 and 12 s after drop deposition are shown in Figure 4.

In spite of the similar chemical composition among samples, WCA varied expressively between them with measured values in the range 52-89° at 0 s. The lowest WCA was found for PBSu BF, which was statistically lower than all the other samples at the initial contact of the water drop (52 ± 8°; $p < 0.001$). Moreover, the WCA for this sample decreased further to 15 ± 4°, 12 s after placement of the water drop. Conversely, the highest WCA was observed for PBSu BF Ctr (89 ± 4°), with no significant changes being observed with time. Finally, WCA of PBSu PL (79 ± 2°) was very similar to PBSu PL Ctr (80 ± 1°) at time 0s, and a small but statistically significant increase in WCA for PBSu PL was sequentially observed 6s and 12 s after deposition of the water drop (compared to the respective WCA at 0s; $p < 0.01$).

The WCA is known to be affected not only by the surface chemistry of the substrate, but also by the presence of nano- or microscale patterns [46]. WCA of substrates prepared by BF is typically higher (lower wettability) than that of flat controls, due to the increased roughness of the surface, and tendency toward air pocket formation [47–49]. In this work, however, the WCA of PBSu BF was the lowest among all samples, which can be explained by the fact that none of the samples was truly flat (as shown by the estimated average pore size, roughness values and topography images), and by the easy penetration of water through the pores of this sample, as supported by the fast decrease in WCA during the 12s, and as discussed previously by others [50,51].

The fact that PBSu BF Ctr, PBSu PL and PBSu PL Ctr were all within a relatively narrow range of WCA values (79-89° at 0s) can be explained by the broadly similar pore size of these samples (1-2 μm). The presence of large regions of the surface with small pores creates the conditions for the entrapment of air pockets under the drop, causing the WCA to increase. Previous studies by Wu and Wang on PCL

honeycomb films containing micrometer-scale pores have similarly shown that higher WCA values can be measured when pore size decreases (in the sequence flat <10 µm < 6 µm < 3.5 µm) [52].

A remark should again be given to emphasize that PBSu BF Ctr indeed contained large areas of such small pore size, albeit its inhomogeneity (Figure 2). In addition, it is interesting to note the contrasting low R value (high diffusion) measured for this material, in spite of the low surface wettability. This is explained by three important facts: a) presence of significantly large pores in some small regions of the sample; b) presence of small but very thin areas in this sample (as low as 4 µm in some regions); and c) the fast measuring time of the WCA determination, and associated small probing region and absence of soaking conditions, as opposed to the R measurements. The data hence suggest that longer and extensive soaking may be needed to eliminate the entrapped air and thereafter increase the wettability and overall permeability of the sample.

In the review by Gigli et al [27], a comparison of WCA of different PBSu-based materials and composites shows that the WCA is dependent on the processing methods employed, resulting in a wide range of values for untreated surfaces, i.e. 50-107° [10,14,27,28,32]. It is interesting to note that small variations in solvent casting conditions (more prominently RH% and presence of surfactant) can also clearly yield different results in terms of WCA, which were particularly noticeable when comparing PBSu BF, BF Ctr and PL or PL Ctr. Conversely, the fact that no significant differences in WCA were found between PBSu PL and PL Ctr at 0 s suggests that no major changes in surface features are created by including the porogen in the polymer solution. The slight decrease in the WCA of PBSu PL with time is, however, suggestive of the easier penetration of water through the pores due to the highest porosity of this sample created by particle leaching. Even so, the fact that the differences between this sample and the control are so small highlights again the drawbacks of the PL method, particularly the difficult production of homogeneous samples with high wettability and/or diffusion properties[41].

3.4. Hydrolytic stability of PBSu films

Results for the *in vitro* degradation profile of PBSu films are shown in Figure 5. In spite of the low sample thickness, films were found to be stable for at least 4 weeks. In most cases, mass loss was small over the 16 week period of the experiment, which is consistent with the low hydrolysis rate of the polymer [27]. Mass loss in PBS BF and PBS BF Ctr was only found significant when the samples were incubated for 16 weeks ($p < 0.05$). For PBSu PL and PBSu PL Ctr, mass loss was found significant at the 4-week and 8-week time points, respectively. The first signs of sample brittleness were observed in most cases after 8 weeks of incubation, and after 16 weeks only PBSu PL Ctr had become expressively fragmented, which explains the absence of data for the sample for that time point. The PBSu BF Ctr films were found to be the most durable and also the easiest to handle, most likely due to the presence of significantly thicker regions in the sample, as shown previously in Figure 3.

Mass loss observed for polymer materials is typically associated with two main events: a) bulk erosion, resulting from the penetration of water molecules through the pores, causing hydrolytic degradation inside the scaffold, and b) surface erosion, caused by the contact of the water molecules with the surface [53].

In order to establish the relationship between surface area and surface erosion, changes in surface roughness during the *in vitro* degradation experiment were assessed by AFM analysis (Supplementary material S1). Surface R_a values (Figure 5 b) generally decreased with incubation time, due to the cleavage of hydrolytically sensitive bonds leading to loss of the polymer from the surface. Because PBS BF and PBSu BF Ctr were the samples with the highest initial surface R_a and highest SA (Table 2), these were also the samples that suffered the most significant surface erosion. AFM images demonstrate more notably that the surface erosion of PBSu BF causes the pores to lose their organized arrangement, likely making visible the lower layers of the matrix, characterized by a more random pore distribution [3]. The fact that this sample was the one that underwent higher surface erosion may also be related with its higher wettability, as estimated from the previously discussed WCA measurements (Figure 4). The data hence supports the hypothesis that samples prepared under humid air flow were mostly subjected to surface erosion, while the

effects of bulk erosion were less prominent, thereby not compromising the *in vitro* stability of these samples.

Differences of R_a with incubation time were not so pronounced for the samples prepared by particulate leaching (PBSu PL), and for the respective control (PBSu PL Ctr). This observation likely results from the fact that these samples were prepared at room humidity, and that the matrix is more uniform across the z-direction, with the exception of the presence of small pores created by particulate leaching. As such, lower layers of the film that become exposed due to erosion reveal similar surface R_a values to the topmost layer, and the differences become poorly significant.

3.5. Viability and adhesion of hESC-RPE

As mentioned previously, hESCs offer an ideal source of RPE in cell therapies, as they can be produced vast amounts *in vitro*. In addition, protocols for differentiation down the RPE lineage using defined and xeno-free conditions have been well established [25], and the differentiated cells have been shown to perform the normal functions of adult RPE [54]. Clinical trials evaluating the therapeutic potential of hESC-RPE in patients suffering from Stargardt's Macular Dystrophy and both forms of Macular Degeneration (dry and exudative) are active or recruiting at the time of writing of this manuscript [55–57].

Porous/patterned films prepared by BF have been increasingly investigated as biomaterials enabling not only cell adhesion and cell growth, but also capable of modulating cell differentiation and gene expression [3]. In this context, cell response is widely acknowledged to be dependent on the physical and chemical properties of the surface, including polymer composition, and the topography of the surface [3]. In the first part of this work, we already established the importance of the surfactant for the formation of the organized array of PBSu BF films, and provided a systematic characterization of the properties of both BF and PL films and their controls. For the cell culture experiments, the attachment and viability of hESC-RPE on porous PBSu PL and BF films was investigated for the first time, and the results are discussed below.

Cell culture studies on the neat PBSu PL and BF surfaces were carried out in parallel with protein-coated equivalents, prepared by pre-immersing the materials in solutions containing collagen type IV and laminin. These ECM proteins are natural components of the basement membrane of the RPE, and are essential for the maturation and differentiation of hESC-RPE [58].

3.5.1. Cell viability/proliferation

Cell proliferation on the uncoated and dip-coated PBS BF and PL films was assessed using the fluorometric resazurin assay (Figure 6). A significant increase in metabolic activity was observed after 5 days for the protein-coated PBS BF, and for the uncoated PBS PL ($p < 0.05$). Differences between the samples at day 1 were not statistically significant at the 95% confidence level. At day 5, the differences started approaching significance, particularly for the dip-coated PBS BF, when compared to the uncoated BF and dip-coated PL ($p = 0.08$).

Examples form the literature show that PBSu substrates can allow the attachment and spreading of different cell types, but nonetheless that cell proliferation can be improved by the presence of ECM proteins [15]. On the other hand, cell viability onto uncoated PBSu substrates can be manipulated by modifying the surface topography, as shown by Coutinho et al who compared PBSu substrates with different groove and ridge sizes prepared by micromolding [59]. In our work, the results show that both the presence of ECM proteins (containing cell adhesion motifs and providing a biomimetic environment) and the presence of a regular surface porosity facilitate the adhesion and proliferation of hESC-RPE. One of the main advantages of porous surfaces is that the pores and rims constitute hooking sites to which cells can attach through extending filopodia [3]. This effect, together with the fact that PBSu BF films had the highest surface area and the lowest WCA (i.e. highest wettability), likely contributed to the improved cell adhesion and proliferation on these surfaces.

3.6. Localization of protein markers

In the native retina, RPE cells express the ECM proteins that compose the Bruch's membrane, namely collagen types I, II, III and IV, as well as laminin and fibronectin. The production of ECM proteins by functional RPE can also be observed *in vitro* when the cells are cultured for as little as 3 days [60]. In our work, we firstly investigated the secretion of laminin, collagen type IV and fibronectin by hESC-RPE, when the cells were cultured on the uncoated PBSu BF and PBSu PL films (first two rows of Figure 7). Expression of the ECM proteins was mostly undetected after 1 day, but became noticeable already after 5 days on PBSu BF, whereas practically no protein expression was detected for uncoated PBSu PL.

In agreement with the cell viability results (Figure 6), cell number was generally increased when cells were seeded on the protein-coated surfaces, as observed by the stained nuclei (last two rows of Figure 7). As expected, laminin and collagen were detected on the coated surfaces, at both day 1 and day 5. These proteins were often found co-localized due to the topographical preference of proteins when they adsorb to the patterned surfaces. The most striking observation was the wide expression of fibronectin by hESC-RPE, which had not been used to coat the materials, particularly on PBSu BF. Small but detectable amounts of fibronectin were additionally secreted by hESC-RPE cultured on uncoated PBSu BF, in spite of the absence of adhesion proteins. This is a very interesting observation if one considers the contrasting results obtained for the uncoated PBSu PL films, where few cells were observed with almost undetected amounts of secreted fibronectin.

Vinculin is a membrane-associated protein which has an essential role in the formation of integrin-mediated adhesions linking the actin cytoskeleton to the ECM. As such, vinculin has become one of the best-characterized proteins of focal adhesions [61]. In this work, actin and vinculin were stained and imaged by confocal microscopy in order to investigate the formation of focal complexes of hESC-RPE cells to the PBSu films (Figure 8). The adherence phenomena of RPE onto surfaces have been widely discussed using cells of non-human origin [62,63], human primary cells [64] and immortalized cell lines [65–67] but, to the best of our knowledge, very little information is available concerning the adhesive behavior of hESC-RPE, and no reports can be found focusing on the adhesion of hESC-RPE onto biodegradable and patterned surfaces.

The uncoated surfaces showed a limited amount of adherent cells, as discussed before, and a generally low presence of actin and vinculin, with the exception of hESC-RPE cultured for 5 days on PBSu BF films. Cells cultured on the dip-coated films showed a higher presence of actin and vinculin right from the first day, and most prominently after 5 days in culture. In addition, cells cultured on coated PBSu BF assumed a spherical morphology after 5 days, showing a localized distribution of focal adhesions, whereas cells cultured on PBSu PL substrates were mostly fibroblast-like, with longer actin filaments and wide distribution of focal adhesions along the cell edge. This is in line with results published by Lim et al [67], who reported that ARPE-19 cells cultivated on smooth surfaces started to spread already after 1 day of culture, whereas cells on micropatterned surfaces were found to retain a round morphology. After 1 and 3 weeks of culture, the cells grown on smooth surfaces showed a multilayer fibrillar cytoskeleton network, while cells on patterned surfaces did not show fibroblast-like phenotypes, and instead expressed a monolayered network of actin stress fibres [67]. It has been reported that less differentiated cells demonstrate a wider focal contact area, in consistency with a strong adhesion, which results in the cells becoming flatter and losing their differentiated RPE morphology [68].

Altogether, our studies support the hypothesis that the different surface properties of the PBSu films, such as topography, specific surface area, roughness and wettability can significantly affect the way cells sense the surface and are able to interact with it, namely during early focal contact. In this context, the porous topography of BF films seemingly favored the proliferation and morphology of the cells, and the secretion of ECM proteins. Even so, additional studies should be carried out in order to establish the effects of the PBSu substrates at later stages of hESC-RPE maturation, including morphological aspects, differentiation, gene expression and function.

Conclusions

In this study, we demonstrated that polybutylene succinate can be processed into porous films by two different solvent casting methods, resulting in materials with very distinct properties, including thickness, diffusion capacity, surface roughness and surface area, and wettability. The BF method effectively produced homogeneous films with a regular porous topography, somewhat resembling a honeycomb-like arrangement. Our preliminary results on the adhesion of hESC-RPE to PBSu films suggest that the early focal contact can be manipulated by tuning the surface properties of the coated PBSu films, with measurable effects on cell viability and morphology, and, expectedly, on other cellular events such as migration, gene expression and differentiation. In our studies, protein-coated PBSu BF films encouragingly promoted cell viability, and supported the early focal adhesion of hESC-RPE cells. Future experiments should explore the versatility of this method to produce films of different thickness and with tunable pore size and pore distribution, having in mind a broader scope of tissue engineering applications.

Acknowledgments

Funding from the Academy of Finland (decision numbers 304909 and 310325) is gratefully acknowledged. The authors also wish to thank our research engineer Suvi Heinämäki, and our laboratory technicians Outi Melin and Hanna Pekkanen for their valuable technical assistance during this work. Finally, the authors are grateful to the Tampere Imaging Facility (BioMediTech, Tampere University) for assisting in the confocal microscopy imaging.

Data availability statement

The raw/processed data required to reproduce these findings cannot be shared at this time as the data also forms part of an ongoing study.

References

1. O'Brien, F. J. Biomaterials & scaffolds for tissue engineering. *Mater. Today* **14**, 88–95 (2011).
2. Fernandez-Yague, M. A. *et al*. Biomimetic approaches in bone tissue engineering: Integrating biological and physicomechanical strategies. *Adv. Drug Deliv. Rev.* **84**, 1–29 (2015).
3. Calejo, M. T., Ilmarinen, T., Skottman, H. & Kellomäki, M. Breath figures in tissue engineering and drug delivery: State-of-the-art and future perspectives. *Acta Biomater.* **66**, 44–66 (2018).
4. Widawski, G., Rawiso, M. & François, B. Self-organized honeycomb morphology of star-polymer polystyrene films. *Nature* **369**, 387–389 (1994).
5. Zhang, A., Bai, H. & Li, L. Breath figure: a nature-inspired preparation method for ordered porous films. *Chem. Rev.* **39**, 510–554 (2015).
6. Muñoz-Bonilla, A., Fernández-García, M. & Rodríguez-Hernández, J. Towards hierarchically ordered functional porous polymeric surfaces prepared by the breath figures approach. *Prog. Polym. Sci.* **39**, 510–554 (2014).
7. Calejo, M. T., Ilmarinen, T., Jongprasitkul, H., Skottman, H. & Kellomäki, M. Honeycomb porous films as permeable scaffold materials for human embryonic stem cell-derived retinal pigment epithelium. *J. Biomed. Mater. Res. A* **104**, 1646–1656 (2016).
8. Calejo, M. T. *et al.* Langmuir-Schaefer film deposition onto honeycomb porous films for retinal tissue engineering. *Acta Biomater.* **54**, 138–149 (2017).
9. Strauss, O. The retinal pigment epithelium in visual function. *Physiol. Rev.* **85**, 845–881 (2005).
10. Wang, H. *et al.* Biocompatibility and bioactivity of plasma-treated biodegradable poly(butylene succinate). *Acta Biomater.* **5**, 279–287 (2009).
11. Wu, Z. *et al.* Effects of magnesium silicate on the mechanical properties, biocompatibility, bioactivity, degradability, and osteogenesis of poly(butylene succinate)-based composite scaffolds for bone repair. *J. Mater. Chem. B* **4**, 7974–7988 (2016).

12. Hariraksapitak, P., Suwantong, O., Pavasant, P. & Supaphol, P. Effectual drug-releasing porous scaffolds from 1,6-diisocyanatohexane-extended poly(1,4-butylene succinate) for bone tissue regeneration. *Polymer* **49**, 2678–2685 (2008).

13. Ojansivu, M. *et al*. Knitted 3D Scaffolds of polybutylene succinate support human mesenchymal stem cell growth and osteogenesis. *Stem Cells Int.* **2018**, (2018).

14. Almeida, L. R. *et al.* New biotextiles for tissue engineering: Development, characterization and in vitro cellular viability. *Acta Biomater.* **9**, 8167–8181 (2013).

15. Abay, N., Gurel Pekozer, G., Ramazanoglu, M. & Kose, G. T. Bone formation from porcine dental germ stem cells on surface modified polybutylene succinate scaffolds. *Stem Cells International* (2016). doi:10.1155/2016/8792191

16. Klimanskaya, I. *et al*. Derivation and comparative assessment of retinal pigment epithelium from human embryonic stem cells using transcriptomics. *Cloning Stem Cells* **6**, 217–245 (2004).

17. Xiang, P. *et al.* A novel Bruch's membrane-mimetic electrospun substrate scaffold for human retinal pigment epithelium cells. *Biomaterials* **35**, 9777–9788 (2014).

18. Shadforth, A. M. A., George, K. A., Kwan, A. S., Chirila, T. V. & Harkin, D. G. The cultivation of human retinal pigment epithelial cells on Bombyx mori silk fibroin. *Biomaterials* **33**, 4110–4117 (2012).

19. Shadforth, A. M. A., Chirila, T. V., Harkin, D. G., Kwan, A. S. L. & Chen, F. K. Biomaterial templates for the culture and transplantation of retinal pigment epithelial cells: A critical review. in *Biomaterials and Regenerative Medicine in Ophthalmology (Second Edition)* (eds. Chirila, T. V. & Harkin, D. G.) 263–289 (Woodhead Publishing, 2016). doi:10.1016/B978-0-08-100147-9.00011-0

20. Hotaling, N. A. *et al*. Nanofiber scaffold-based tissue-engineered retinal pigment epithelium to treat degenerative eye diseases. *J. Ocul. Pharmacol. Ther.* **32**, 272–285 (2016).

21. Sorkio, A. E. *et al.* Biomimetic collagen I and IV double layer Langmuir–Schaefer films as microenvironment for human pluripotent stem cell derived retinal pigment epithelial cells. *Biomaterials* **51**, 257–269 (2015).

22. Subrizi, A. *et al*. Generation of hESC-derived retinal pigment epithelium on biopolymer coated polyimide membranes. *Biomaterials* **33**, 8047–8054 (2012).

23. Rowland, T. J. *et al*. Differentiation of human pluripotent stem cells to retinal pigmented epithelium in defined conditions using purified extracellular matrix proteins. *J. Tissue Eng. Regen. Med.* **7**, 642–653 (2013).

24. Vaajasaari, H. *et al*. Toward the defined and xeno-free differentiation of functional human pluripotent stem cell-derived retinal pigment epithelial cells. *Mol. Vis.* **17**, 558–575 (2011).

25. Hongisto, H., Ilmarinen, T., Vattulainen, M., Mikhailova, A. & Skottman, H. Xeno- and feeder-free differentiation of human pluripotent stem cells to two distinct ocular epithelial cell types using simple modifications of one method. *Stem Cell Res. Ther*. **8**, 291 (2017).

26. Skottman, H. Derivation and characterization of three new human embryonic stem cell lines in Finland. *Vitro Cell. Dev. Biol. - Anim.* **46**, 206–209 (2010).

27. Gigli, M. *et al*. Poly(butylene succinate)-based polyesters for biomedical applications: A review. *Eur. Polym. J*. **75**, 431–460 (2016).

28. Li, H., Chang, J., Cao, A. & Wang, J. In vitro evaluation of biodegradable poly(butylene succinate) as a novel biomaterial. *Macromol. Biosci.* **5**, 433–440

29. Yang, J., Tian, W., Li, Q., Li, Y. & Cao, A. Novel biodegradable aliphatic poly(butylene succinate-co-cyclic carbonate)s bearing functionalizable carbonate building blocks: II. Enzymatic biodegradation and in vitro biocompatibility assay. *Biomacromolecules* **5**, 2258–2268 (2004).

30. Gualandi, C. *et al*. Easily synthesized novel biodegradable copolyesters with adjustable properties for biomedical applications. *Soft Matter* **8**, 5466–5476 (2012).

31. Correlo, V. M. *et al*. Properties of melt processed chitosan and aliphatic polyester blends. *Mater. Sci. Eng. A* **403**, 57–68 (2005).

32. Coutinho, D. F. *et al*. The effect of chitosan on the in vitro biological performance of chitosan-poly(butylene succinate) blends. *Biomacromolecules* **9**, 1139–1145 (2008).

33. McMillan, J. R. *et al.* Small-diameter porous poly (ε-caprolactone) films enhance adhesion and growth of human cultured epidermal keratinocyte and dermal fibroblast cells. *Tissue Eng*. **13**, 789–798 (2007).

34. Ponnusamy, T., Chakravarty, G., Mondal, D. & John, V. T. Novel 'breath figure'-based synthetic PLGA matrices for in vitro modeling of mammary morphogenesis and assessing chemotherapeutic response. *Adv. Healthc. Mater.* **3**, 703–713 (2014).

35. Foldberg, S. *et al.* Patterned poly(lactic acid) films support growth and spontaneous multilineage gene expression of adipose-derived stem cells. *Colloids Surf. B Biointerfaces* **93**, 92–99 (2012).

36. Wu, B.-H. *et al.* Self-assembly of patterned porous films from cyclic polystyrenes via the breath figure method. *J. Phys. Chem. C* **122**, 3926–3933 (2018).

37. Liu, Q. *et al*. Honeycomb-patterned porous films fabricated via self-organization of Tb complex-loaded amphiphilic copolymers. *RSC Adv.* **8**, 19524–19531 (2018).

38. Wang, W. *et al*. Static miscible vapor environment controlled honeycombed morphology in polystyrene–b–poly(methyl methacrylate) films. *Polymer* (2018). doi:10.1016/j.polymer.2018.07.037

39. Zhang, H. *et al.* Synthesis of novel guanidine-based ABA triblock copolymers and their antimicrobial honeycomb films. *Polym. Chem.* **9**, 3922–3930 (2018).

40. Vargas-Alfredo, N. *et al*. Fabrication of biocompatible and efficient antimicrobial porous polymer surfaces by the Breath Figures approach. *J. Colloid Interface Sci.* **513**, 820–830 (2018).

41. Liao, C.-J. *et al*. Fabrication of porous biodegradable polymer scaffolds using a solvent merging/particulate leaching method. *J. Biomed. Mater. Res.* **59**, 676–681 (2002).

42. Komez, A., Baran, E. T., Erdem, U., Hasirci, N. & Hasirci, V. Construction of a patterned hydrogel—fibrous mat bilayer structure to mimic choroid and Bruch's membrane layers of retina. *J. Biomed. Mater. Res. A* n/a-n/a (2016). doi:10.1002/jbm.a.35756

43. Nishikawa, T. *et al*. Micropatterns based on deformation of a viscoelastic honeycomb mesh. *Langmuir* **19**, 6193–6201 (2003).

44. Escalé, P., Rubatat, L., Billon, L. & Save, M. Recent advances in honeycomb-structured porous polymer films prepared via breath figures. *Eur. Polym. J.* **48**, 1001–1025 (2012).

45. Fukuhira, Y., Yabu, H., Ijiro, K. & Shimomura, M. Interfacial tension governs the formation of self-organized honeycomb-patterned polymer films. *Soft Matter* **5**, 2037–2041 (2009).

46. Yuan, Y. & Lee, T. R. Contact Angle and Wetting Properties. in *Surface Science Techniques* 3–34 (Springer, Berlin, Heidelberg, 2013). doi:10.1007/978-3-642-34243-1_1

47. Chen, J., Yan, X., Zhao, Q., Li, L. & Huang, F. Adjustable supramolecular polymer microstructures fabricated by the breath figure method. *Polym. Chem.* **3**, 458–462 (2012).

48. Bui, V.-T. *et al*. Ordered honeycomb biocompatible polymer films via a one-step solution-immersion phase separation used as a scaffold for cell cultures. *Chem. Eng. J.* **320**, 561–569 (2017).

49. Mongkhontreerat, S. *et al.* Functional porous membranes from amorphous linear dendritic polyester hybrids. *Polym. Chem.* **6**, 2390–2395 (2015).

50. Stenzel, M. H., Barner-Kowollik, C. & Davis, T. P. Formation of honeycomb-structured, porous films via breath figures with different polymer architectures. *J. Polym. Sci. Part Polym. Chem.* **44**, 2363–2375 (2006).

51. Min, E., Wong, K. H. & Stenzel, M. H. Microwells with patterned proteins by a self-assembly process using honeycomb-structured porous films. *Adv. Mater.* **20**, 3550–3556 (2008).

52. Wu, X. & Wang, S. Regulating MC3T3-E1 cells on deformable poly(ε-caprolactone) honeycomb films prepared using a surfactant-free breath figure method in a water-miscible solvent. *ACS Appl. Mater. Interfaces* **4**, 4966–4975 (2012).

53. Asli, M. M., Pourdeyhimi, B. & Loboa, E. G. Release profiles of tricalcium phosphate nanoparticles from poly(L-lactic acid) electrospun scaffolds with single component, core-sheath, or porous fiber morphologies: effects on hASC viability and osteogenic differentiation. *Macromol. Biosci.* **12**, 893–900 (2012).

54. Leach, L. L. & Clegg, D. O. Making stem cells retinal: methods for deriving retinal pigment epithelium and implications for patients with ocular disease. *Stem Cells Dayt. Ohio* **33**, 2363–2373 (2015).

55. Belfort Jr, R. Stem Cell Therapy for Outer Retinal Degenerations - ClinicalTrials.gov. Available at: https://clinicaltrials.gov/ct2/show/NCT02903576. (Accessed: 19th October 2018)

56. ZhengQin, Y. Clinical Study of Subretinal Transplantation of Human Embryo Stem Cell Derived Retinal Pigment Epitheliums in Treatment of Macular Degeneration Diseases - ClinicalTrials.gov. Available at: https://clinicaltrials.gov/ct2/show/NCT02749734. (Accessed: 19th October 2018)

57. Astellas Institute for Regenerative Medicine. A Follow up Study to Determine the Safety and Tolerability of Sub-retinal Transplantation of Human Embryonic Stem Cell Derived Retinal Pigmented Epithelial (hESC-RPE) Cells in Patients With Stargardt's Macular Dystrophy (SMD) - ClinicalTrials.gov. Available at: https://clinicaltrials.gov/ct2/show/NCT02941991. (Accessed: 19th October 2018)

58. Sorkio, A. *et al*. Structure and barrier properties of human embryonic stem cell-derived retinal pigment epithelial cells are affected by extracellular matrix protein coating. *Tissue Eng. Part A* **20**, 622–634 (2014).

59. Coutinho, D. F., Gomes, M. E., Neves, N. M. & Reis, R. L. Development of micropatterned surfaces of poly(butylene succinate) by micromolding for guided tissue engineering. *Acta Biomater.* **8**, 1490–1497 (2012).

60. Campochiaro, P. A., Jerdon, J. A. & Glaser, B. M. The extracellular matrix of human retinal pigment epithelial cells in vivo and its synthesis in vitro. *Invest. Ophthalmol. Vis. Sci.* **27**, 1615–1621 (1986).

61. Atherton, P., Stutchbury, B., Jethwa, D. & Ballestrem, C. Mechanosensitive components of integrin adhesions: Role of vinculin. *Exp. Cell Res.* **343**, 21–27 (2016).

62. Opas, M. The focal adhesions of chick retinal pigmented epithelial cells. *Can. J. Biochem. Cell Biol.* **63**, 553–563 (1985).

63. Opas, M. & Kalnins, V. I. Light-microscopical analysis of focal adhesions of retinal pigmented epithelial cells. *Invest. Ophthalmol. Vis. Sci.* **27**, 1622–1633 (1986).

64. Parapuram, S. K. *et al.* Differential effects of TGFbeta and vitreous on the transformation of retinal pigment epithelial cells. *Invest. Ophthalmol. Vis. Sci.* **50**, 5965–5974 (2009).

65. Lee, K. *et al*. Contribution of actin filaments and microtubules to cell elongation and alignment depends on the grating depth of microgratings. *J. Nanobiotechnology* **14**, 35 (2016).

66. Baldwin, A. K. *et al*. Epithelial–mesenchymal status influences how cells deposit fibrillin microfibrils. *J Cell Sci* **127**, 158–171 (2014).

67. Lim, J.-M. *et al.* Retinal pigment epithelial cell behavior is modulated by alterations in focal cell–substrate contacts. *Invest. Ophthalmol. Vis. Sci*. **45**, 4210–4216 (2004).

68. Opas, M., Turksen, K. & Kalnins, V. I. Adhesiveness and distribution of vinculin and spectrin in retinal pigmented epithelial cells during growth and differentiation in vitro. *Dev. Biol.* **107**, 269–280 (1985).

Figures

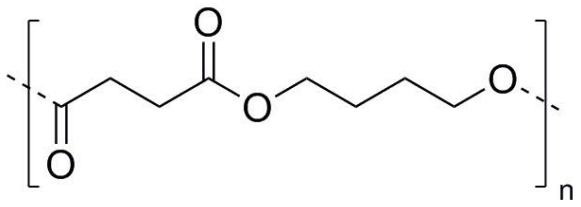

Figure 1. Chemical structure of PBSu.

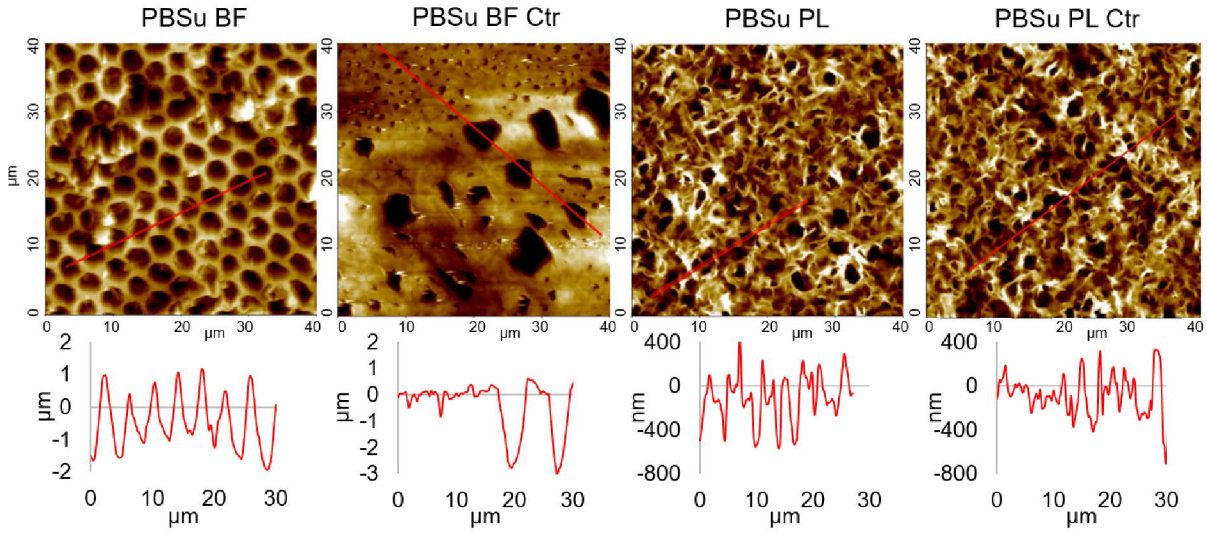

Figure 2. AFM images of PBSu films prepared by the BF and PL methods, and respective controls (prepared respectively in the absence of DOPE and sucrose particles, according to the compositions shown in Table 1). Plots shown under the AFM images denote the height topographical profiles across the red lines shown in the AFM images.

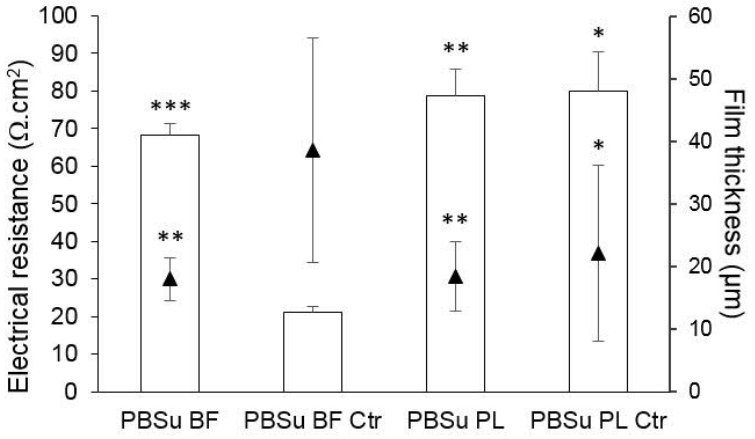

Figure 3. Electrical resistance (R) of PBSu films prepared by BF and PL methods, and respective controls (columns, left vertical axis). The average thickness of the films is shown as the triangular markers (right vertical axis). Statistical differences found in relation to PBSu BF Ctr are indicated above the columns (R) and markers (thickness). * $p < 0.05$, ** $P < 0.01$, *** $p < 0.001$.

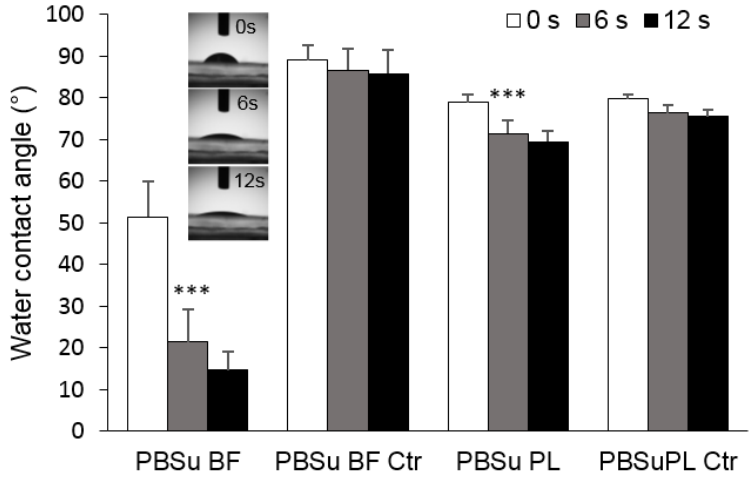

Figure 4. WCA of PBSu films in the 12 seconds following drop deposition. *** $p < 0.001$ compared to the preceding time point. The inset in the figure shows the water droplets deposited onto PBSu BF and the modification of contact angle after 6 and 12 s.

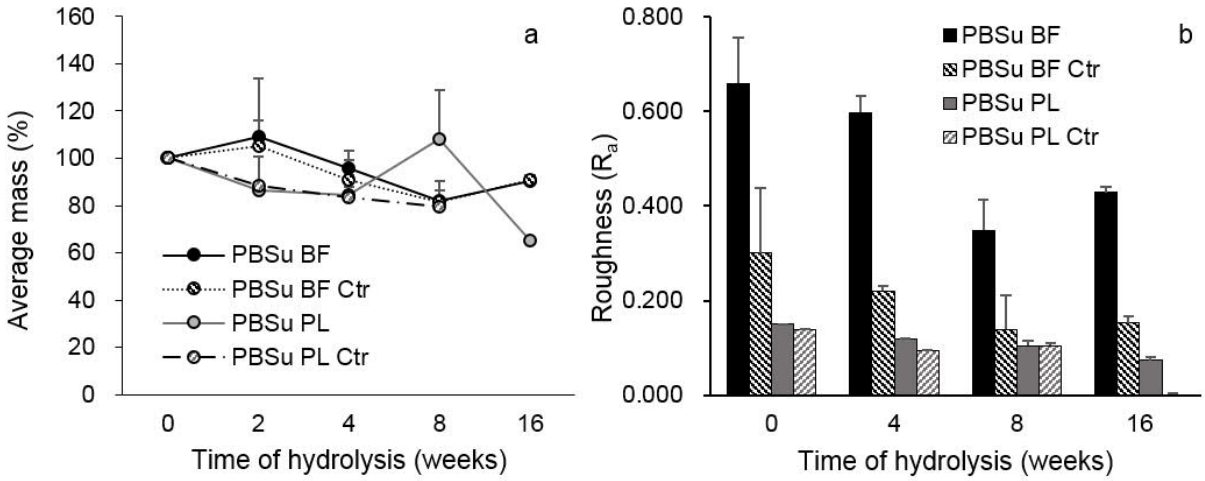

Figure 5. Average mass (a) and surface roughness (R_a) of PBSu films during immersion in TRIS-buffer for 16 weeks. Data for the 16 week time point for PBSu PL Ctr is absent due to film break-up after the long incubation period.

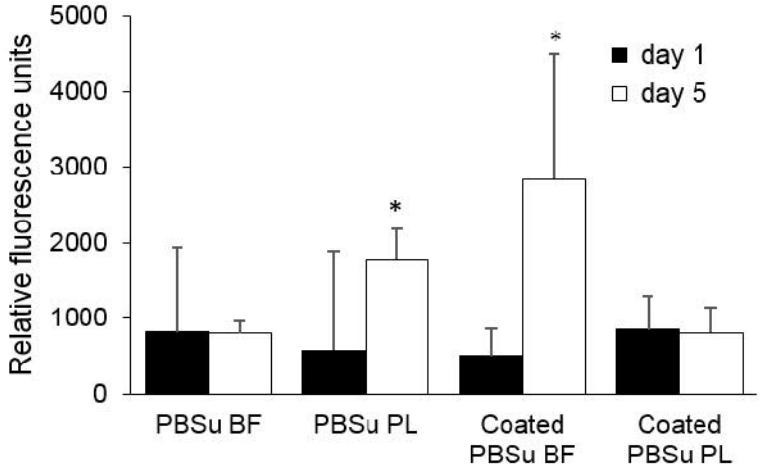

Figure 6. Relative fluorescence units indicative of hESC-RPE proliferation on the uncoated and dip-coated films. * $p < 0.05$ compared to the same sample cultured for one day.

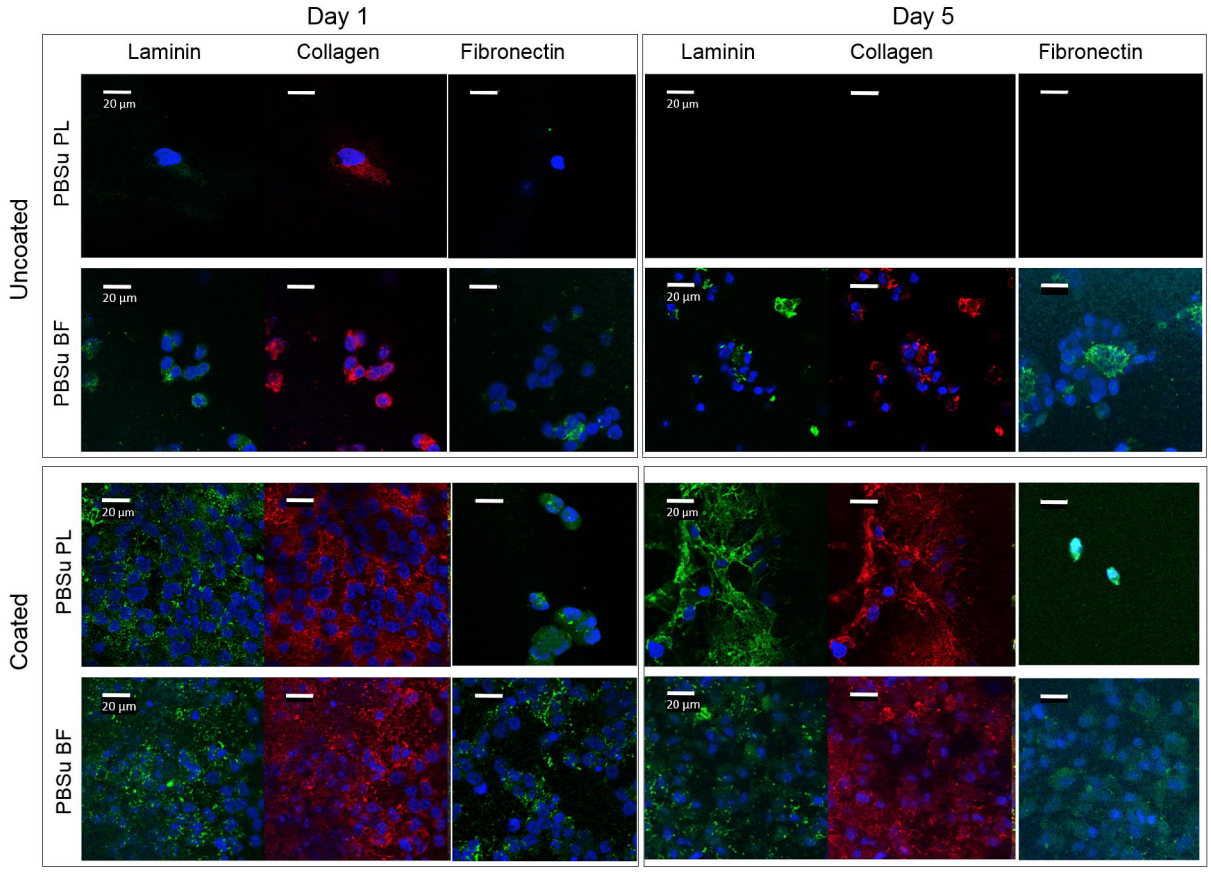

Figure 7. Confocal microscopy images showing the localization of laminin (green), collagen type IV (red) and fibronectin (green) on uncoated and dip-coated PBSu BF and PBSu PL films after 1 and 5 days. DAPI-stained nuclei are shown in blue. Scale bar = 20 µm.

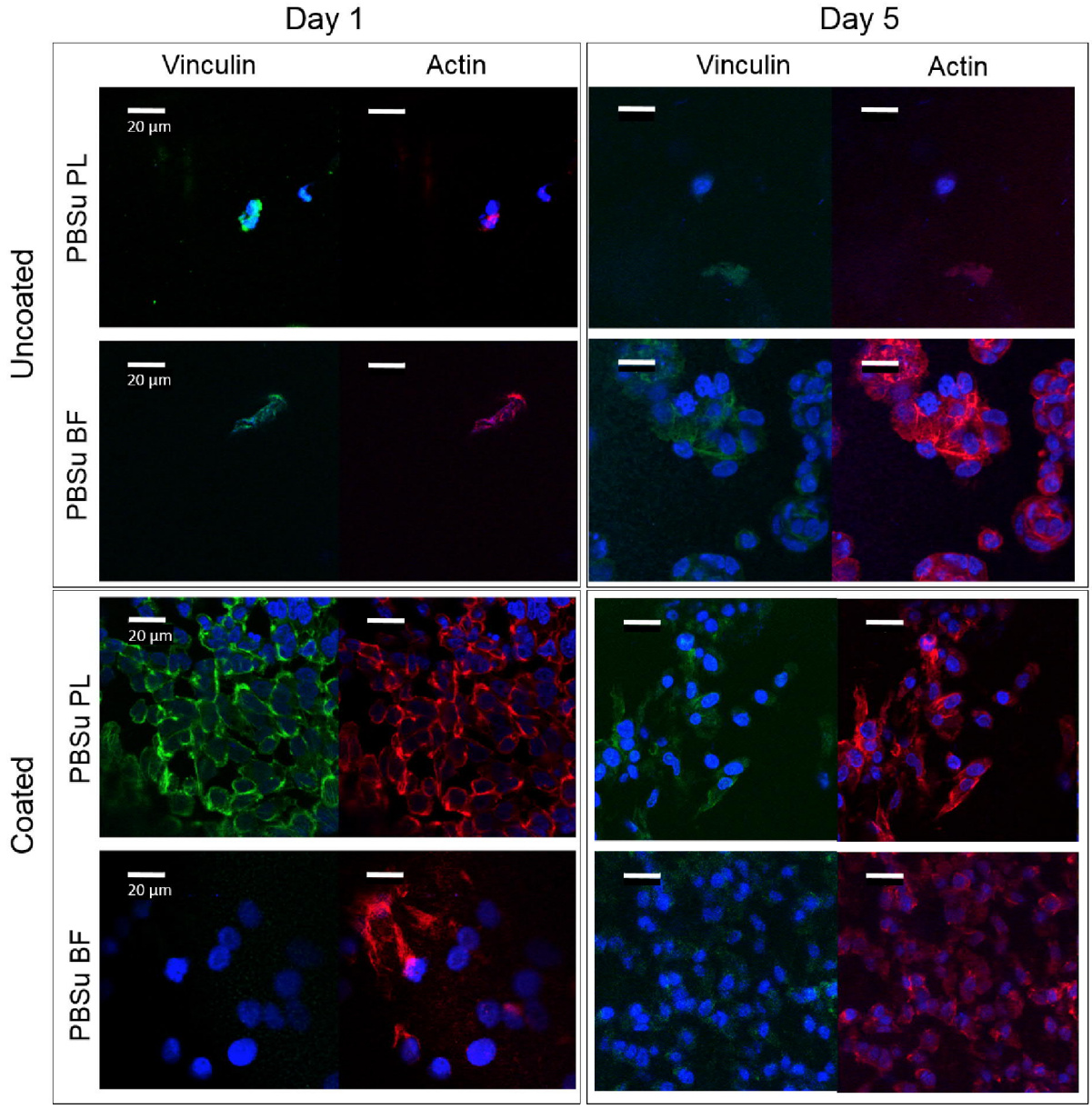

Figure 8. Confocal microscopy images showing the localization of vinculin (green) and actin (red) on uncoated and dip-coated PBSu BF and PBSu PL films after 1 and 5 days. DAPI-stained nuclei are shown in blue. Scale bar = 20 µm.

Supplementary material

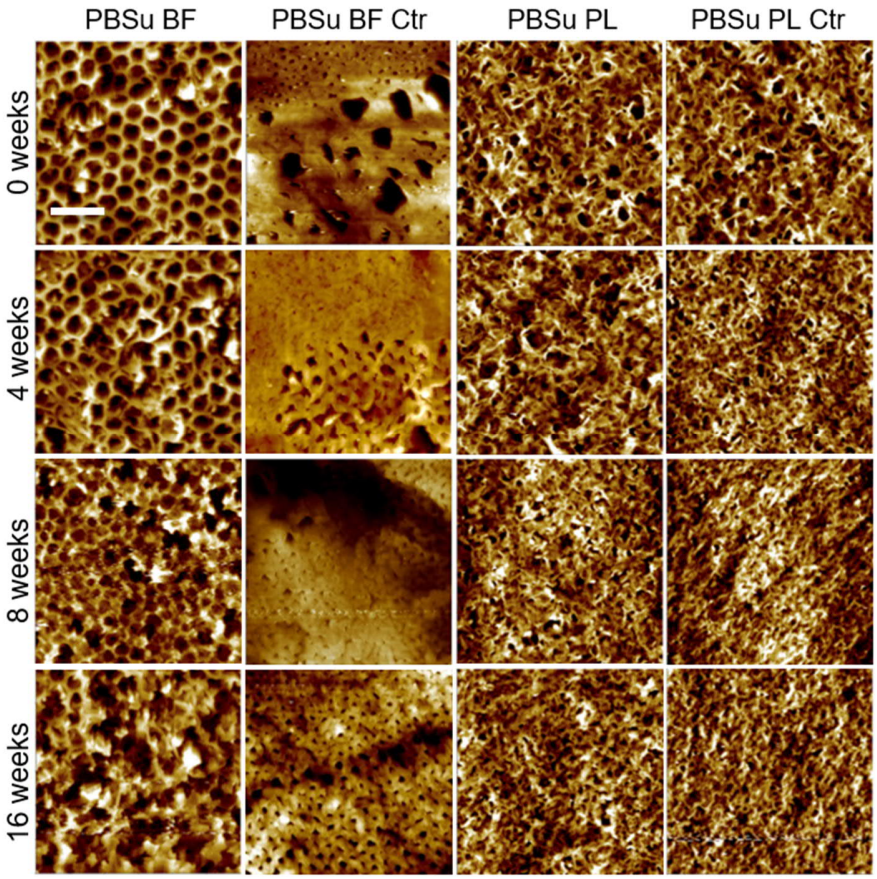

S1. AFM images showing the surface topography of PBSu films following in vitro hydrolysis for different time periods. Scale bar: 10 µm.

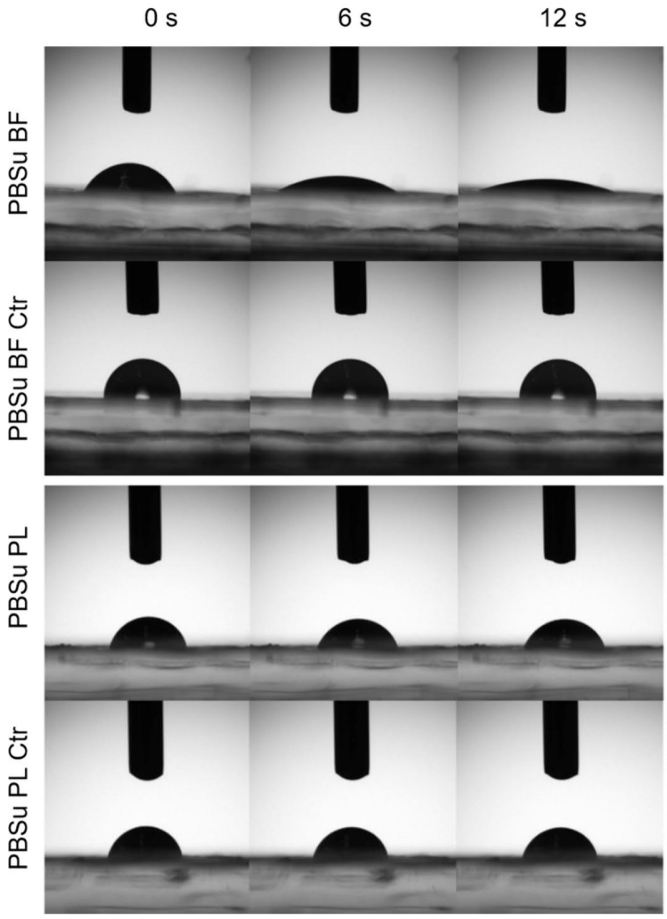

S2. Optical microscopy images of water drops in contact with the surface of the films, acquired during WCA measurements.